Covalency in semiconductor quantum dots

CHEMICAL SOCIETY REVIEWS

James R. Heath and Joseph J. Shiang

UCLA Department of Chemistry and Biochemistry, 405 Hilgard Avenue, Los Angeles, California 90095-1569 USA

Chemical schemes for the preparation of direct band-gap semiconductor quantum dots have advanced rapidly over the past few years. It is now possible to prepare a variety of III–V semiconductors with a finite size (InP, InAs, GaAs, *etc.*) and compare their size-dependent properties with the well studied II–VI class of quantum dots (ZnS, CdS, CdSe, *etc.*). In this Review, various physical properties of semiconductor quantum dots are presented within a discussion framework of lattice covalency. Included in the Review are discussions of the various chemical synthetic routes for making the particles, as well the electronic structure and the electronic dynamics of nanocrystals.

1 Introduction

Crystalline solids are typically characterized by various physical properties such as melting point, conductivity, color, *etc.* However, each of these physical properties has a characteristic length scale, generally of the order of 10–100 nm or so. If the physical limits of the crystal are reduced below the characteristic length scale for a particular property, then that property becomes 'size confined'. In this case, the property is no longer just a function of the chemical and structural nature of the material, but also of the size and shape of the crystal. In the past decade, the modification of materials characteristics by size and shape control has been demonstrated for a host of technologically important metallic and semiconducting solids.[1] Although all crystalline materials can, in principle, exhibit finite-size effects, perhaps the most spectacular examples of size-confinement have been observed in nanocrystals (or quantum dots) of inorganic semiconducting solids. The number of size-dependent phenomena that have been observed in semiconductor quantum dots include light emission from Si nanocrystals and porous Si,[2] broad band-gap tunability in the direct gap semiconducting nanoparticles,[3] and size-dependent structural phase diagrams and melting points.[4] This remarkable range of size-dependent properties that are available from chemically similar systems have made semiconducting nanoparticles attractive candidates for many technological applications. For example, nanocrystals can be size-tuned to behave as wavelength specific photoemitters or photoabsorbers for light emitting diode (LED) or photovoltaic applications, respectively.[1] Another potential application takes advantage of the fact that the energies of the photo-generated positive and negative charge carriers within a particle are also size-tunable. Thus, various applications in which particles are used as energy selective photo-oxidative or -reductive catalysts have been explored.[5] Other possible applications are related to electrically charging nanocrystals. The energy to electrically charge a nanocrystal is size-dependent, and for particles less than 10 nm in size, this charging energy is substantially larger than kT at room temperature. Thus, several groups have explored using nanocrystals as single-electron capacitive or switching devices.[6] At this date, however, large-scale applications of semiconducting nanocrystals have yet to emerge, and the study of these materials is still most appropriately referred to as 'nanoscience', rather than 'nano-technology'.

The chemical techniques for controlling nanocrystal size, and the accompanying development of a physical picture of finite size effects, began in the early 1980s with Brus' pioneering work on solution-phase synthesized II–VI quantum dots.[7] Since that time, a steady series of advances in the chemical preparation of these nanocrystals have made II–VI nanocrystals the prototypes for the investigation of finite size effects. The wide variety of II–VI nanocrystals available has enabled

James R. Heath is Professor of Chemistry at UCLA. As a graduate student in 1985, he was a co-discoverer of the fullerenes, along with Richard Smalley, Robert Curl, and Sir Harold Kroto and Sean O'Brien. He received his PhD in 1988 and took a Miller Fellowship at UC Berkeley. At Berkeley, he worked with Richard Saykally, developing spectroscopic techniques for probing the structures of bare clusters of refractory elements. In 1991 he joined the research staff at IBM Watson Labs, and, in 1994, he moved to UCLA, taking the position of assistant professor. He was promoted to Associate Professor in 1996, and Professor in 1997. His current research interests center on building nanoscale architectures for computational applications.

James R. Heath

Joseph Shiang received his bachelor's degree from the California Institute of Technology in 1988. He received his PhD (Chemistry) in 1994 from the University of California, Berkeley while working under the direction of A. Paul Alivisatos and was a Postdoctoral associate at the University of California, Los Angeles from 1995 to 1997. His scientific interests are in the use of spectroscopic methods, and in particular, their application to nanoscale systems. He is currently at the Center for Ultrafast Optical Sciences at the University of Michigan, Ann Arbor.

Joseph Shiang

researchers to establish periodic trends within the II and VI columns of the periodic table (*i.e.* ZnSe *vs.* CdTe). Until recently, it has not been possible to explore periodic trends within rows of the periodic table. Moving along rows within the periodic table (toward III–V or Group IV materials) increases the covalent character of the chemical bonding, and thus should have profound impact on size-dependent properties. In the past few years synthetic schemes have been developed for fabricating Group IV (Si,[2,8] Ge[9]) and III–V (InP,[10,11] InAs,[12] GaP,[10] GaAs[13]) semiconducting materials in finite size. Of these two classes of materials, the III–Vs are the most closely related to the II–VIs. Like the II–VIs, most III–Vs are direct gap semiconductors. They are also characterized by tetrahedral bonding geometries (wurtzite or zinc blende crystal habits), and the chemical nature of the unit cell has both ionic and covalent bonding contributions. The availability of high-quality, size-selected III–V nanocrystals has enabled various chemical and physical characterizations of finite-size effects in these materials. The purpose of this review is to use the language of lattice covalency to compare the size-dependent properties of a typical III–V nanocrystal system, InP, with those of the best understood II–VI nanocrystal systems, CdSe and/or CdS. In Section 2, we present a basic picture of the electronic structure of a nanocrystal, emphasizing briefly the similarities and the differences that exist between various semiconductors. In Section 3, we will show that the covalency of the nanocrystal lattice is reflected in the relative level of difficulty in preparing high quality, size-selected nanocrystals of these materials. In Section 4, we discuss how lattice covalency affects the various electronic length scales in these quantum dots, including the size of the electron and hole wavefunctions, and the length and time scales associated with electron-phonon coupling and short time-scale excited electronic state dephasing. In Section 5, we discuss how lattice covalency is reflected in the nature of observed surface electronic states, and how this impacts long time-scale excited electronic state relaxation processes. Finally, recent developments related to the inorganic passivation of the surface states for both types of nanocrystals will be discussed.

2 Electronic wavefunctions in semiconductor nanocrystals

Excellent articles concerning the size-dependence of the electronic states in semiconductor nanocrystals have appeared in the recent literature,[1,14,15] and so only a very brief discussion will be presented here, with a focus on the importance of covalent interactions in quantum size effects. Further details will be provided as need in Sections 4 and 5.

A reasonable picture of finite size effects in semiconductor nanocrystals can be gained by considering the energy band representation of a simple one-electron, one-dimensional semiconductor, such as that shown in Fig. 1. Each unit cell is represented by a lattice constant a, and contains a single p_z-orbital with a unit cell energy of E. The energy level diagram is essentially that expected from Huckel theory, where β is the electronic overlap integral between adjacent unit cells. The lowest energy state will correspond to the situation in which there exists a bonding interaction between neighboring unit cells. A cartoon diagram is shown at the bottom right of Fig. 1. Note that all of the p-orbitals have the same orientation with respect to one another—*i.e.* in ‘real’ space’ they are all ‘in phase’. In reciprocal, or $\mathbf{k}$-space, this corresponds to the $\mathbf{k} = 0$ state, and it has an energy $E - \beta$. At the bottom right of Fig. 1 is shown a representation in which each unit cell has a net antibonding interaction with each of its neighbours, and the phase of any given p-orbital is rotated by 180° (or π) with respect to the neighboring unit cells. In $\mathbf{k}$-space, this corresponds to $\mathbf{k} = \pi/a$, and the energy of this state equals $E + \beta$. The imposition of finite size modifies this picture in several ways. First, the continuous curve drawn in Fig. 1 implies an infinite 1D solid. In any *finite* solid, the curved line correlating the wavevector $\mathbf{k}$ with energy is non-continuous, only containing as many points as there are unit cells in the solid. Second, the largest wavefunctions are those near $\mathbf{k} = 0$, and, in a finite sized crystal, such wavefunctions will no longer fit within the physical dimensions of the crystallite. Thus, as the particle size is reduced, the distribution of energy levels with respect to $\mathbf{k}$ becomes discrete, and the $\mathbf{k}$-values corresponding to the largest size wavefunctions (near $\mathbf{k} = 0$) are removed first. If the semiconductor were a direct-gap material, then the lowest energy allowed transition would be at $\mathbf{k} = 0$, from the top of the valence band (VB) to the bottom of the conduction band (CB). In a tetrahedral semiconductor, the orbitals at the top of the valence band are the p-orbitals, which are threefold degenerate at $\mathbf{k} = 0$. The s-orbital is at the bottom of the conduction band. The imposition of finite size would affect the lowest energy optical transitions by moving them to higher energy (by removal of the lowest $\mathbf{k}$ states). This is shown in the circular inset of Fig. 1. In addition, rather than an absorption spectrum that is a continuum above the band gap energy, the absorption spectrum would now be composed of discrete states, since $\mathbf{k}$ itself is discrete.

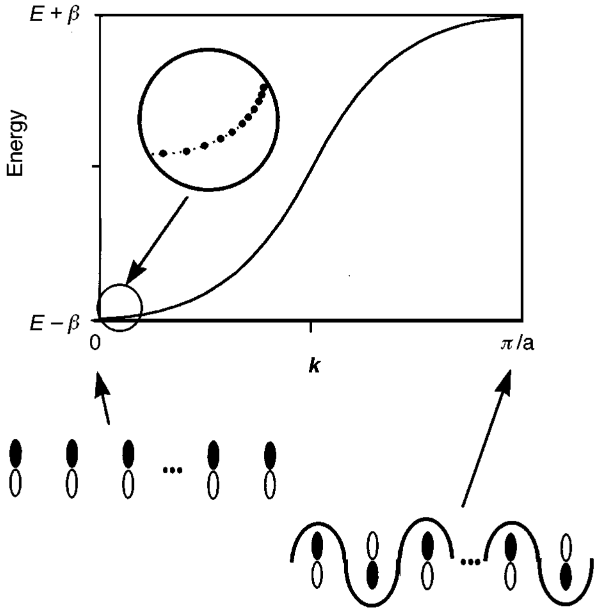

Fig. 1 Band structure of a one dimensional solid containing only a single π-bonding p-orbital. The energy width of the band is a measurement of the amount of covalent bonding in the unit cell. For a bulk crystal, the energy band is continuous, but for a finite-sized (nano)crystal, the band is discrete, containing only as many points as there are unit cells in the crystal. An example of this is shown in the circular inset. The wavefunctions near $\mathbf{k} = 0$ are the largest wavefunctions in this solid, and are therefore first removed by the imposition of finite size.

Relevant to this review is the issue of how increased covalent bonding manifests itself in finite size effects. Of primary importance is the width of the energy bands ($= 2\beta$ in Fig. 1), a quantity which is directly proportional to the amount of covalent bonding in the solid. Strongly ionic solids are characterized by flat (and narrow width) energy bands. This translates into a large uncertainty in $\mathbf{k}$ with respect to energy, and therefore localized electronic wavefunctions. Covalent solids, on the other hand, are characterized by broad, highly curved energy bands and delocalized wavefunctions. A measurement of the curvature of an energy band, and thus a measurement of the amount of delocalization of the corresponding wavefunctions, is the effective mass, m^* ($= h^2/8\pi^2\beta a^2$) of electrons (or holes) in those states, where h is Planck’s constant, and a is the unit cell lattice constant.[16] For a few II–VI and III–V direct gap semiconductors, the ratio of m^* to the mass of an electron, m_e, is CdS ($= 0.20$), CdSe ($= 0.13$), InP ($= 0.13$) and InAs (0.039).[17] To some extent, lighter carrier masses also correlate to narrower energy gaps, and the energy gaps for these same four semiconductors are CdS ($= 2.56$ eV), CdSe (= 1.84 eV), InP (= 1.42 eV) and InAs (= 0.42 eV).[17] Parameters which are of equal importance to m^* in considering finite size effects, and which are even more strongly correlated to the amount of covalent bonding in the lattice, are the static and optical relative permittivity (ε_0 and ε_∞). ε_∞ describes the response of the lattice valence electrons to an applied electric field. ε_0 describes the response of *both* the valence electrons and the cationic and anionic cores, and is thus larger than ε_∞. For a homoatomic material, where all nuclei have same effective charge, the two constants are the same. In homoatomic metals, where bonding is completely covalent and electrons are delocalized, ε is, of course, inifinite. In large band gap insulators, on the other hand, ε_∞ is typically < 6 or so, indicating that charge carriers are poorly screened from the ionic cores. The tendency of ε_∞ to increase with increasing covalency is demonstrated by considering a series of solids, ranging from I–VII to Group IV materials: CuCl (= 5.7), CdS (= 5.2), CdSe (= 5.8), InP (= 9.6), InAs (= 12.3), and Ge (= 16.0).[17]

In a direct gap semiconductor, the first excited state is an electron–hole pair, or an exciton, which has a radius, that, from a simple Bohr atom picture, is given by $r_{\mathrm{exc}} = \{\varepsilon^*/(m^*/m_e)\}a_o$, where a_o is the Bohr radius.[18] The relative permittivity here is denoted as ε^* because, in general, one cannot use either ε_0 or ε_∞ directly. In an exciton, the electron and the hole are screened from one another by both the lattice cores and the valence electrons. If an exciton is small (the highly ionic I–VIIs fall into this category), then the charge carriers move much faster than the characteristic vibrational frequency of the lattice, and only the valence electrons contibute to the screening. Thus, $\varepsilon^* = \varepsilon_\infty$. However, in more covalent materials (such as III–Vs), the exciton is relatively large and is screened by both the ionic cores and the valence electrons, and thus $\varepsilon^* = \varepsilon_0$. II–VI semiconductors are intermediate, and ε^* has contributions from both constants. The upshot of this argument is that III–Vs are characterized by much larger exciton radii than the more ionic II–VIs. For example, in CdSe $r_{\mathrm{exc}} = 35$ Å, and in InP, $r_{\mathrm{exc}} = 70$ Å. The exciton radius is the most important length scale in determining at what particle diameter 'finite size' effects become important. When the size of the crystallite lattice is decreased below the exciton radius, quantum size effects appear in the room temperature electronic and optical properties. Other length scales, such as the respective sizes of the negative and positive charge carrier wavefunctions, become important at smaller sizes. According to the simple physical models presented in this section, the degree of covalent bonding in the semiconductor lattice determines both the onset and the magnitude of finite size effects. Thus, for the semiconducting materials discussed here, finite size effects should be more pronounced in III–V nanocrystals.

3 Synthesis of II–VIs and III–Vs

There are many ways to produce semiconductor quantum dots, ranging from gas-phase photolysis/thermolysis of inorganic precursors,[2,8] to growing quantum dot 'islands' *via* heteroepitaxy,[19] to inorganic and organo-metallic solution-phase synthetic schemes for producing quantum dot colloids.[1] These various approaches all have advantages. The gas-phase techniques are very general, and the heteroepitaxial techniques are relatively consistent with semiconductor processing technology. The colloidal syntheses produce particles that are most amenable to the various characterization techniques familar to most chemists. In addition, the highest quality particles, in terms of narrow size distribution and defect-free crystal structures, have been produced by these solution-phase routes. It is these particles that we will focus on here. The ideal nanocrystal synthesis produces particles that are soluble, monodisperse, and characterized by a (chemically controllable) narrow size distribution. In 1951 Reiss showed that in order to produce a narrow size distribution of a given type of particle, it was necessary to temporally separate the particle nucleation and growth steps.[20] He showed that if the nucleation step could be carried out within some discrete time window, δt, and the particles then grown by a diffusion-controlled growth mechanism for a given time t_g, then the width of the particle size distribution would be determined by both δt and t_g. If narrow distributions are required for very small particles, then it is necessary to keep δt as short as possible. Although this concept is easy to visualize, it can be very difficult to put into practice. Murray *et al.* showed that, for the II–VI class of nanocrystals, nucleation and growth could be temporally separated, and that very narrow distributions of monodisperse nanocrystals could be readily prepared in the size range from 15–150 Å.[3] From a chemical point of view, it is the nature of the II–VI nanocrystal precursors that allow for such a reaction scheme. In a typical synthesis, bare ions or atoms are directly reacted with each other at high temperature (~350 °C) *via* rapid injection of one reagent [*e.g.* Me_2Cd dissolved in trioctylphosphine (TOP)] into a flask containing a hot (300 °C) solution of equimolar amounts of another (*e.g.* a solution of Se metal dissolved in a TOP–trioctylphosphine oxide (TOPO) solution). Both of the solvents, TOP and TOPO are coordinating solvents that are stable to very high temperatures. Particle nucleation is initiated immediately upon injection. During the injection process, sufficient volume (of the Me_2Cd–TOP solution) is added such that the temperature of the reacting mixture drops below 180 °C, thereby stopping particle nucleation within seconds. The flask is slowly raised to above 200 °C to allow for particle growth. After a predetermined time period, the reaction is quenched and the product nanocrystals are precipitated and purified. This reaction, or variations thereof, can be utilized to produce extremely narrow distributions of many II–VI nanocrystals. Subsequent size-narrowing techniques, such as solvent pair precipitation, can be utilized to further narrow the product size distribution to the point where all particles are virtually identical when viewed by transmission electron microscopy (TEM).

In a successively more covalent series of materials, it becomes increasingly difficult to separate the nucleation and growth processes. This is due both to the nature of the reagents used to make the particles, and to the nature of the particles themselves. For the III–V and Group IV systems, bare atoms or ions are not chemically stable species, and so the reactions to produce nanocrystals must be carried out with strongly complexed precursors. Because of this, particle nucleation and growth are both high temperature processes, and it is difficult to separate the two. For the II–VI, III–V, and Group IV semiconductors, the ground state structure is crystalline. However, for the more covalent of these materials, amorphous structural phases become increasingly important, and are typically formed more easily at lower temperatures. Consider, for example, the series of semiconductors CdS, InP and Ge. It is possible to grow CdS nanocrystals at room temperature[21] (although not by the method described above), and only moderate annealing temperatures are required to produce high quality nanocrystals. InP nanocrystals, however, require temperatures in the range of 250 °C or so, and such temperatures must be maintained for a several day annealing period to obtain high quality nanocrystals. Finally, the temperatures and times required to make Ge nanocrystals are near 300 °C for several days, with most of this time again devoted to crystallite annealing.

Because of the high temperatures and long times required for producing III–V nanocrystals, it is not possible to obtain a narrow distribution from a single synthesis, and particles sizes must be selected after the synthesis is complete. Nevertheless, certain similarities do exist between III–V and II–VI synthetic schemes. Most notably is the use of the coordinating solvent TOPO, in concert with the dehalosylation reactions developed by Wells' group.[22] In a typical synthesis, a TOPO–$InCl_x$ complex is prepared by heating a flask of $InCl_3$ dissolved in TOPO at 100 °C for several hours. An equal molar amount of tris(trimethylsilyl)phosphine is injected, and the temperature is slowly raised to ~ 260 °C and maintained at that temperature for several days. The temperature of the flask is lowered to 100 °C, and an excess of an alkylamine (dodecylamine, for example) is injected. The final product consists of InP nanocrystals, capped with a mixture of TOPO and alkylamine, and characterized by a size distribution ranging from 15–50 nm. All steps are carried out using Schlenk lines and other standard airless procedures. The final product InP nanocrystals may be size separated by dissolving the particles into toluene. A series of steps are then carried out in which small aliquots of methanol or acetone are added to the stirring toluene/particle solution, and the solution is filtered. The dried precipitate is then redissolved in a non-polar organic solvent such as hexane or toluene. The largest particles precipitate from the solution first. In this manner, up to 40 spectroscopically unique (as measured by the optical absorption edge) size distributions may be extracted from a single synthesis.[11] Several UV–VIS spectra, taken from a much larger precipitation series from a single reaction, are shown in Fig. 2. Particle sizes, as measured by various microscopic and diffraction techniques, are indicated next to a couple of the absorption curves.

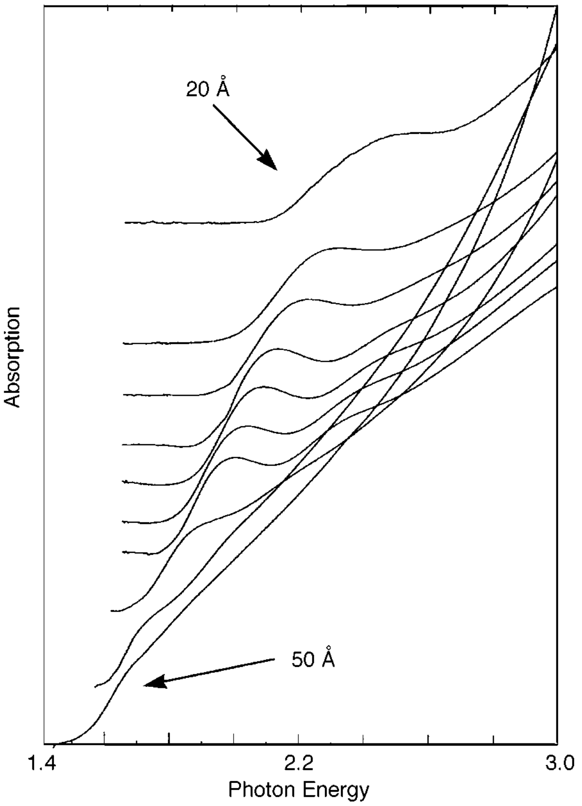

Fig. 2 Absorption spectra of a series of InP nanocrystal colloids, size selected from a single synthetic product mixture. Adapted from Ref. 11.

4 The first excited electronic state: short time scale dynamics

In Section 2, a simple description for size confined wave functions in semiconductor nanocrystals was presented, and the quantization of the energy level spacing with respect to wavevector (***k***) was discussed. An implication of this picture is that the band gap absorption oscillator strength for the bulk solid is collapsed into a few discrete transitions. In sufficiently narrow distributions of II–VI quantum dots, such discrete transitions have been observed and, more recently, spectroscopically assigned.[23] The nature of the lowest lying band gap transitions in finite sized solids is particularly important for photonics-related applications, and much effort has been expended toward trying to measure the natural linewidths and short-time scale relaxation dynamics in semiconducting nanocrystals. In this section of the review, we present a brief overview of this picture, and we pay special attention to how the nature of covalent *vs.* ionic lattice interactions affects short-time scale dynamics. Section 5 will deal with longer-time scale carrier relaxation processes.

In a bulk (direct-gap) semiconducting solid, optical excitation across the band gap produces two charge carriers of opposite sign, an electron (e^-) and a hole (h^+). At finite temperature, the dominant relaxation mechanism of the initially prepared state is provided by interactions between the charge carriers and lattice vibrations. These lattice vibrations are described in the next paragraph. Such a scattering mechanism is intrinsic to the material, while other secondary processes, such as scattering at defects or dopant sites, are extrinsic. With the imposition of finite size, new intrinsic and extrinsic mechanisms can become important. For example, charge carrier scattering at the particle boundaries is an intrinsic mechanism, and is, of course, expected to exhibit a particle size dependence. Charge carrier scattering or trapping by surface states or nanocrystal defects are extrinsic mechanisms, which can potentially be removed by appropriate nanocrystal chemical (surface) passivation and crystallite annealing. Over the past few years, several groups have addressed, both theoretically[24] and experimentally, excited state charge-carrier dynamics on short time scales. Experimentally, probes such as temporal[25] and spectral hole burning, single particle spectroscopy,[26] femtosecond two- and three-pulse photon-echo experiments,[27] and resonance Raman spectroscopy,[28] have provided much information about the various fast relaxation processes. This is a very complex topic and not completely understood. Only a brief discussion of the points most salient to the degree of crystallite lattice covalency will be discussed here.

The bulk, solid state analogues of molecular vibrations are lattice phonons. These phonons come in two flavors—low frequency acoustic modes (< 50 cm^{-1}) and higher frequency optical modes (300–800 cm^{-1}). Both the acoustic and optical phonons can be classified by two types of lattice motion. Longtitudinal modes (LO and LA modes for optical and acoustic phonons, respectively) are symmetric, breathing type motions. Transverse modes (TO and TA) are twisting-like motions. As is the case with molecules, these vibrations can couple to excited electronic states, and such coupling can provide mechanisms for excited electronic state relaxation. The coupling of these various types of modes to excited state charge carriers is not equivalent. It turns out that the primary mechanism for the initial relaxation (dephasing) of an excited charge carrier is through the longtitudinal acoustic (LA) phonons, mediated through what is known as deformation potential coupling. When a charge carrier is placed on a lattice site, there is an accompanying dilation of the lattice around the charge carrier. This dilation affects the electronic wavefunction overlap between adjacent atoms in the neighborhood of the charge, and thus alters the energy levels of the corresponding electronic states. This coupling between lattice distortion and electron energy levels is deformation potential coupling, and it is mediated by the LA phonons.

The following analogy is useful when extending this picture of electron–phonon coupling in semiconductor nanocrystals. When an electron is excited across the band-gap, it is moved from a bonding to an anti-bonding orbital, and thus one net bond is broken. This ‘broken bond’, however, is distributed over several unit cells (the exciton volume). With the imposition of finite size, however, the broken bond becomes more localized, and so the accompanying lattice dilatation has a larger amplitude. Alivisatos *et al.* have developed a mathematical formalism for relating deformation potential coupling to a finite sized particle.[25] This picture relies heavily on the elastic constants of a sphere, and, as will be discussed below, the covalency of the lattice enters into this formalism through these constants.

If the ground and excited electronic states are assumed to have harmonic oscillator potential forms, then the offset between the lowest energy vibrational states ($v = 0$) of the two wells is given by Δ_{ac}, where the 'ac' subscript implies that the vibrational levels correspond to acoustic phonons. Δ_{ac} is given by:

$$\Delta_{ac} = [0.97^2 (D_e - D_h)^2] [\pi R^3 C_{11} h\omega_{ac}]^{-1} \quad (1)$$

where $D_e - D_h$ is the acoustic mode deformation potential, and C_{11} is the elastic constant, and R is the radius of the crystallite. The acoustic mode frequency is given by $\omega_{ac} = (\zeta_{ac}/R)v_s$, where v_s is the sound velocity and ζ_{ac} is a mathematical root designed to make the acoustic mode wavefunction vanish at the crystallite boundary.[29] Combining this expression for ω_{ac} with eqn. 1, one finds a net R^{-2} dependence in the offset Δ_{ac}. At high temperatures, eqn. 1 leads to the following expression for the excited state dephasing rate:[30]

$$\Phi(t) = \exp\{\pi\omega \Delta^2 k_b T t^2)/h\} \quad (2)$$

In eqn. 2, T is temperature, k_b is Boltzmann's constant and h is Planck's constant. The degree of covalency within the semiconductor quantum dot enters into this rate expression in a few ways. One might expect, based on its physical description, that the deformation potential is strongly coupled to covalency. In fact, Harrison has shown that, within a tight binding picture of the band structure, a formalism based on electronic overlap between nearest neighbors in the crystal can be used to determine the deformation potential.[31] However, he also points out that, while such an approach yields reasonable answers, there is no clear correlation between the deformation potential and covalency, probably because of the difficulty in obtaining accurate experimental values of the deformation potential. However, the C_{11} elastic constant is a measurement that relates how volume changes in the unit cell alter the electronic energy of the solid. It is therefore a sensitive function of covalency, and can be accurately measured and calculated. Experimentally determined values of C_{11} for various semiconductors are (in 10^{11} dynes cm^{-2}): Si (16.6), InP (10.11), CdS (8.3), and CdSe (7.41).[17] This value enters into the rate equation (2) as $\exp(C_{11}{}^{-2})$. Arguments based on lattice covalency will thus predict that (at finite temperatures) the more covalent the nanocrystal lattice, the faster the excited state dephasing time. In all cases, the dephasing times should shorten substantially as particle size is decreased. Note that the scattering of charge carriers off the nanocrystal surface is an important additional dephasing process for all particles, independent of the nature of the lattice.

In Figs. 3 and 4 we present two complementary pieces of experimental data in which the excited state dephasing rate is measured as a function temperature for a single size (Fig. 3) and as a function of size for a single temperature (Fig. 4). Fig. 3 (from Ref. 32) represents a direct measurement of this rate as probed by femtosecond 3-pulse photon echo experiments on 29 Å InP and CdSe nanocrystals.[27] Also included in Fig. 3 is a curve, based on the intrinsic effects accounted for by eqn. 3, to model both the InP and CdSe data. Fig. 4 (from Ref. 28) represents an indirect probe of the same process. Here, the ratios of the experimentally determined Raman scattering cross sections for the LO and TO modes of InP nanocrystals are presented as a function of particle size. It is not intuitively obvious that the resonance Raman experiment should measure the same dephasing dynamics that are measured by the time-domain experiments. It turns out that the LO and TO modes are coupled to the excited state potential surface in different manners and are 90° out of phase. The TO mode intensity is maximum at the instant of electronic excitation. The LO mode has zero intensity at the moment of optical excitation, and reaches a maximum at one half the LO mode period. Because of this, the ratio of the two observed phonon intensities serves as an indicator of the short time-scale exciton dephasing dynamics. For short dephasing lifetimes, the LO : TO intensity ratio is small. In Fig. 4 a theoretical calculation (not a fit) of the resonance Raman intensity ratios, in which eqn. 2 is explicitly included, is presented with the data. Both the experiment and the theory indicate that the LO mode is suppressed in small size, implying that the dephasing lifetime shortens with decreasing particle size. Although the TO phonon is not observed in finite sized CdSe nanocrystals, resonance Raman LO phonon overtone spectra of CdSe quantum dots has been correlated with exciton dephasing dynamics in that system as well.[27] Those experiments provide further supporting evidence for the picture presented here.

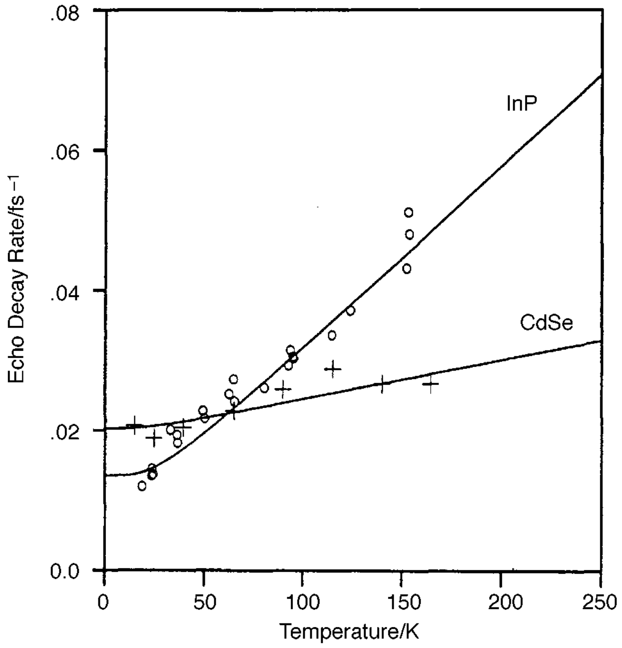

Fig. 3 The temperature dependence of the dephasing rate for 29 Å InP and CdSe nanocrystals, as measured by femtosecond photon echo experiments. Adapted from Reference 32.

5 The first excited electronic state: long time scale dynamics

In Section 4, short time-scale exciton dynamics were dephasing processes that could be discussed largely in terms of the intrinsic properties of nanocrystals, such as the particle size, the deformation potential, and the elastic constants. For these same particles, the long-time scale exciton recombination kinetics are dominated by extrinsic properties of the particles, such as

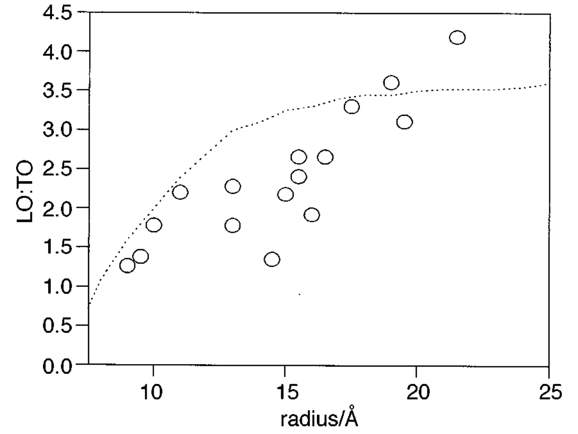

Fig. 4 The ratio of the LO : TO phonon intensities (circles) as a function of particle size. The line is a time-dependent quantum mechanical calculation that utilizes the experimentally determined dephasing rate (from Fig. 3), together with a model describing the size-dependence of electron–phonon coupling in semiconductor quantum dots. This experiment is the frequency-space analogue of the data shown in Fig. 3, although plotted as a function of size, rather than temperature. Adapted from Reference 28.

surface passivation. In large part this is due to the fact that the synthetic techniques discussed in Section 3 are non-ideal. The solubility requirement imposed upon these nanocrystals means that bulky organic ligands are used to passivate the nanocrystal surface. The bulkiness of the ligand is important for solubility, but it also leads to a particle surface that is incompletely passivated. The SiO_2 passivated Si nanocrystals produced by Brus' group have largely circumvented this problem, although the size distribution of those particles is not near the state-of-the-art for II–VIs or even III–Vs. Furthermore, the very recent development of inorganic passivation techniques is beginning to improve the properties of both II–VI and III–V nanocrystals, and such techniques will be briefly discussed at the end of this section. However, for the particles that are discussed in this review, the surface passivation is incomplete, and this has a primary affect on the room-temperature exciton recombination kinetics.

The electron energy level spectrum of III–V and II–VI particles can be modelled as a three-level system, such as that presented in Fig. 5. Although the details of exciton recombination kinetics are complex and have not been completely worked out, a few basic facts have emerged.[33,34,35] Photoexcitation initially places an electron in an (interior) conduction band (CB) state. At temperatures near 0 K, CB-edge luminescence provides the primary mechanism for exciton recombination. Trapping of the excited state electron to a surface state is a slightly activated process, and, at some finite temperature, such trapping begins to dominate the photophysics. Above a few degrees kelvin, the surface states provide a reservoir for nearly all subsequent band-edge or surface state emission processes. Band-edge emission, then, proceeds through an activated 'detrapping' mechanism, which returns an electron from a surface state back to the CB edge. Thus, the nature of the surface states can play a determining role in the observed photoluminescence efficiency at room temperature. The activation barriers for detrapping are determined largely by the depth of the surface states with respect to the CB. These barriers are much greater than the barriers for trapping. This means that band edge luminescence quantum yields will decrease exponentially with increasing depth of the surface state energy levels. It is here that issues relevant to covalency play an important role. Increased ionic bonding character within a bulk crystal leads to successively shallower surface traps. For the relatively ionic II–VI class of materials, the case of surface states on bulk ZnO has been well studied. According to Luth,[36] the presence of the surface (termination of the bulk periodic potential), and the effects of surface reconstruction, are only weak perturbations when compared to the strong ionic forces which dominate the bonding. Thus, the surface states remain very shallow.

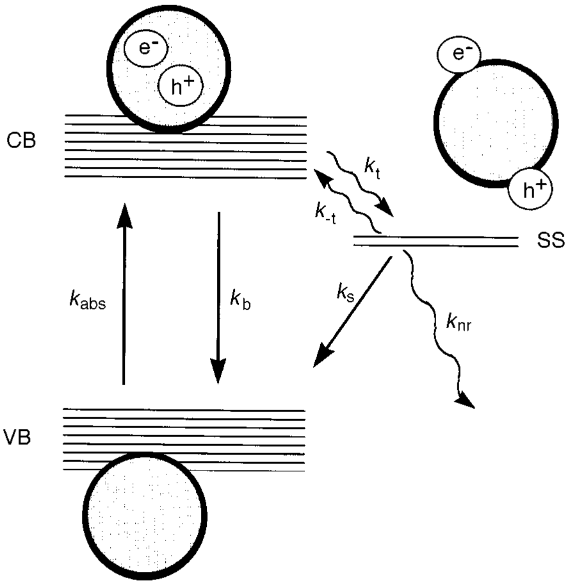

Fig. 5 The three-level system used to describe exciton recombination kinetics in semiconductor nanocrystals. All radiative pathways are indicated by straight arrows, and all non-radiative pathways are indicated by curved arrows. The surface trapping process (indicated by the rate constant k_t, dominates the observed room temperature photophysics.

By measuring the temperature dependence and temporal decay curves of both the band-edge luminescence and surface state luminescence in semiconductor quantum dots, it is possible to measure the activation barrier to surface state detrapping, and thus obtain estimates for the depth of surface states in such systems. The reported values for the depth of the surface states do indeed exhibit a strong dependence on the covalency of the lattice. For 32 Å CdSe nanocrystals surface trap depths are about 0.25 kJ mol^{-1}. For similar sized InP nanocrystals (30 Å), we have found trap depths a full factor of 20 larger (6.3 kJ mol^{-1}). The size dependence of the depth of the surface states depends on the coupling of the surface states to the bulk electronic wave functions. Weaker coupling leads to a stronger size dependence: as the conduction band shifts to higher energy (with decreasing size), the surface states remain behind, and thus become deeper traps with decreasing particle size. As particle size increases from 30 Å to 49 Å, the trap depth in InP nanocrystals is observed to decrease to approximately 3.6 kJ mol^{-1}.

In the introduction of this review, the potential of using semiconductor quantum dots for photonics-based devices was discussed. Such applications typically require high quantum yields for photo- or electro-luminescence efficiency. At first thought, one might expect high luminescence efficiencies from semiconductor quantum dots: the overlap between the electron and hole wavefunctions should be excellent, especially for the smallest particles. However, surface trapping of the carriers greatly reduces photoluminescence quantum yields, such that at room temperature the observed yields for II–VIs are typically only a few percent. For III–Vs the situation is much worse—quantum yields are reduced to only a few hundredths of a percent.

One of the most exciting advances in semiconductor quantum dot syntheses has been the very recent development of inorganic passivation techniques. Although several variations on this theme exist, of particular importance for various photonics-based applications are structures which are characterized by the energy level diagram shown in Fig. 6. The diagram and the cartoon representation of a nanocrystal are intended to describe a quantum dot in which a higher bandgap semiconductor has been grown epitaxially on the surface. Because of the similarities between this system and the well known quantum well systems (GaAs–$Al_xGa_{(1-x)}As$, for example), this type of quantum dot is often called a quantum dot/quantum well (QD/QW). This quantum dot system has, in principle, all of the surface passivation problems that organically passivated quantum dots have. However, separating the low-band gap nanocrystal core from the surface states is a higher band gap semiconductor shell. This high-band gap shell effectively cuts off the radiationless processes that lead to surface trapping, and the lowest energy recombination pathway is not radiationless relaxation from a surface state, but rather charge-carrier recombination within the nanocrystal core, accompanied by photoemission. Examples of such systems include CdSe on ZnS,[37,38] or CdS on InP. Reports of room temperature quantum yields nearing unity have appeared in the recent literature for II–VI on II–VI QD/QWs.

6 Conclusions

Over the last few years, synthetic techniques for producing nearly any type of semiconductor quantum dot have been reported. The properties of these structures are complex, depending on the size, shape, and stoichiometry of the

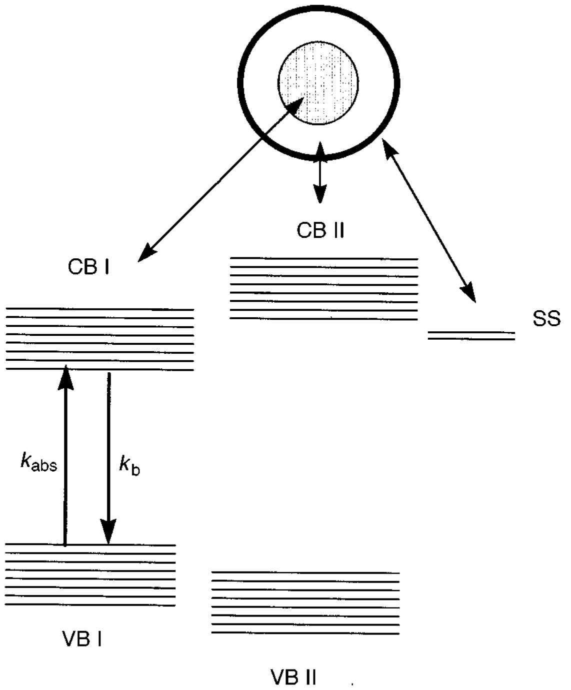

Fig. 6 Energy level diagram of a quantum dot/quantum well system in which a high band semiconductor material has been grown epitaxially onto the surface of a lower band gap semiconductor quantum dot. The higher band gap material forces exciton recombination to occur in the core of the nanocrystal, thus resulting in dramatic increases in photoluminescence efficiency.

nanocrystal. The richness of the available physical and chemical properties have made quantum dots appealing candidates for a variety of applications, and thus it has become important to develop a self-consistent physical picture which can explain and predict those properties. The II–VI class of nanocrystals have been the prototypes for the investigation of size-dependent phenomena, and a detailed picture capable of describing and predicting such phenomena has emerged over the past dozen years or so. With the more recent development of chemical syntheses for producing size-selected III–V nanocrystals, it has become possible to carry out detailed comparisons of the size-dependent properties of one class of particles with another. In this Review, the properties of II–VI and III–V nanocrystals have been rationalized in terms of lattice covalency. While the physical description of III–V nanocrystals is far from complete, arguments based on lattice covalency go a long way toward explaining differences observed with respect to particle synthesis, electronic structure, and electronic dynamics.

7 Acknowledgements

Much of the work described here was carried out by an excellent group of postdocs and graduate students, including Sang-Ho Kim, Rolf Wolters, and Dr Caroline Arnold. Furthermore, a long-time collaboration with the group of Professor Paul Alivisatos is gratefully acknowledged. The work was funded by the NSF-NYI program, a David and Lucille Packard Fellowship, a Dreyfuss Fellowship, and through the Lawrence Berkeley Laboraty Molecular Design Institute, supported by the Office of Naval Research, Order No. N00014-95-F-0099 and by the Director, Offrice of Energy Research, Office of Basic Energy Research, Division of Materials Sciences, of the US Dept. Of Energy under Contract No. DE-AC03, 76SF00098.

8 References

1 For recent reviews, see: (*a*) A. P. Alivisatos, *J. Phys. Chem.*, 1996, **100**, 13 226; (*b*) M. G. Bawendi, M. L. Steigerwald and L. E. Brus, *Ann. Rev. Phys. Chem.*, 1990, **41**, 477.
2 L. E. Brus, *J. Phys. Chem.*, 1994, **98**, 3575.
3 C. B. Murray, D. J. Norris and M. G. Bawendi, *J. Am. Chem. Soc.*, 1993, **115**, 8706.
4 S. H. Tolbert and A. P. Alivisatos, *Ann. Rev. Phys. Chem.*, 1995, **46**, 595.
5 M. R. Hoffman, S. T. Martin, W. Choi and D. W. Bahnemann, *Chem. Rev.*, 1995, **95**, 69.
6 See, for example, G. Markovich, D. V. Leff, S. W. Chung and J. R. Heath, *Appl. Phys. Lett.*, 1997, **70**, 3107 and references therein.
7 N. Chestnoy, T. D. Harris, R. Hull and L. E. Brus, *J. Phys. Chem.*, 1986, **90**, 3393.
8 P. E. Batson and J. R. Heath, *Phys. Rev. Lett.*, 1993, **71**, 911.
9 (*a*) J. R. Heath, J. J. Shiang and A. P. Alivisatos, *J. Chem. Phys.*, 1994, **101**, 1607; (*b*) J. R. Heath and F. K. LeGoues, *Chem. Phys. Lett.*, 1993, **208**, 263.
10 O. I. Micic, J. R. Sprague, C. J. Curtis, K. M. Jones, J. L. Machol, A. J. Notik, H. Giessen, B. Fluegel, G. Mohs and N. Peyghambarian, *J. Phys. Chem.*, 1995, **99**, 7754.
11 A. A. Guzelian, J. E. B. Katari, A. V. Kadavanich, U. Banin, K. Hamad, E. Juban, A. P. Alivisatos, R. H. Wolters, C. C. Arnold and J. R. Heath, *J. Phys. Chem.*, 1996, **100**, 7212.
12 A. A. Guzelian, U. Banin, A. V. Kadavanich, X. Peng and A. P. Alivisatos, *Appl. Phys. Lett.*, 1996, **69**, 1432.
13 M. A. Olshavsky, A. N. Goldstein and A. P. Alivisatos, *J. Am. Chem. Soc.*, 1990, **112**, 9438.
14 N. A. Hill and K. B. Whaley, *Chem. Phys.*, 1996, **210**, 117.
15 L. E. Brus, A. L. Efros and T.Itoh, *J. Lumin.*, 1996, **70**, R7.
16 A derivation of m^* in terms of b is presented in: L. Brus, *New J. Chem.*, 1987, **11**, 123.
17 Landolt-Bornstein, New Series, ed. K. H. Hellwege, Group III, vol. 17a, 1982, Springer-Verlag, Berlin.
18 J. I. Pankove, in *Optical Processes in Semiconductors*, 1987, Dover, New York, p. 9.
19 G. Medeiros-Ribeiro, F. G. Pikus, P. M. Petroff and A. L. Efros, *Phys. Rev. B*, 1997, **55**, 1568.
20 H. Reiss, *J. Chem. Phys.*, 1951, **19**, 482.
21 H. Weller, *Angew. Chem., Int. Ed. Engl.*, 1996, **35**, 1079.
22 R. L. Wells, S. R. Aubuchon, S. S. Kher, M. S. Lube and P. S. White, *Chem. Mater.*, 1995, **7**, 793.
23 A. I. Ekimov, F. Hache, M. C. Schanne-Klein, D. Ricard, C. Flytzanis, I. A. Kudryavsev, T. V. Yazeva, A. V. Rodina and Al. L. Efros, *J. Opt. Soc. Am. B*, 1993, **10**,. 100.
24 T. Takagahara, *Phys. Rev. Lett.*, 1993, **71**, 3577.
25 A. P. Alivisatos, A. L. Harris, N. J. Levinos, M. L. Steigerwald and L. E. Brus, *J. Chem. Phys.*, 1988, **89**, 4001.
26 M. Nirmal, B. O. Dabbousi, M. G. Bawendi, J. J. Macklin, J. K. Trautman, T. D. Harris and L. E. Brus, *Nature*, 1996, **383**, 802.
27 D. Mittleman, R. W. Schoevlein, J. J. Shiang, V. L. Colvin, A. P. Alivisatos and C. V. Shzuk, *Phys. Rev. B*, 1994, **49**, 14 435.
28 J. J. Shiang, R. H. Wolters and J. R. Heath, *J. Chem. Phys.*, 1997, **106**, 8981.
29 S. Nomura and T. Kobayashi, *Solid State Commun.*, 1992, **82**, 335.
30 R. A. Harris, R. A. Mathies and W. T. Pollard, *J. Chem. Phys.*, 1986, **85**, 3744.
31 An excellent book which relates covalent bonding to the properties of bulk, crystalline semiconductors, is: W. A. Harrison, *Electronic Structure and the Properties of Solids*, 1989, Dover, London.
32 U. Banin, G. Cerullo, A. A. Guzelian, C. J. Bardeen, A. P. A. Alivisatos and C. V. Shzuk, *Phys. Rev. B*, 1997, **55**, 7059.
33 A. Eychmuller, A. Hasslebarth, L. Katsikas and H. Weller, *J. Lumin.*, 1991, **48**, 745.
34 (*a*) M. G. Bawendi, W. L. Wilson, L. Rothbert, P. J. Carroll, T. J. Jedju, M. L. Steigerwald and L. E. Brus, *Phys. Rev. Lett.*, 1990, **65**, 1623; (*b*) M. G. Bawendi, P. J. Carroll, W. L. Wilson and L. E. Brus, *J. Chem. Phys.*, 1992, **96**, 946.
35 See S.-H. Kim, R. H. Wolters and J. R. Heath, *J. Chem. Phys.*, 1996, **105**, 7957 and references therein.
36 H. Luth, *Surfaces and Interfaces of Solids*, 1993, Springer, New York.
37 A. R. Kortan, R. Hull, R. L. Opila, M. G. Bawendi, M. L. Steigerwald, P. J. Carroll and L. E. Brus, *J. Am. Chem. Soc.*, 1990, **112**, 1327.
38 M. Danek, K. F. Jensen, C. B. Murray and M. G. Bawendi, *Chem. Mater.*, 1996, **8**, 73.

Received, 21st May 1997
Accepted, 24th September 1997